

Spatially Multi-conditional Image Generation

Ritika Chakraborty^{*1} Nikola Popovic^{*1}, Danda Pani Paudel¹,
Thomas Probst¹, Luc Van Gool^{1,2}

¹ Computer Vision Laboratory, ETH Zurich, Switzerland

² VISICS, ESAT/PSI, KU Leuven, Belgium

{critika, nipopovic, pauDEL, probstt, vangool}@vision.ee.ethz.ch

Abstract. In most scenarios, conditional image generation can be thought of as an inversion of the image understanding process. Since generic image understanding involves the solving of multiple tasks, it is natural to aim at the generation of images via multi-conditioning. However, multi-conditional image generation is a very challenging problem due to the heterogeneity and the sparsity of the (in practice) available conditioning labels. In this work, we propose a novel neural architecture to address the problem of heterogeneity and sparsity of the spatially multi-conditional labels. Our choice of spatial conditioning, such as by semantics and depth, is driven by the promise it holds for better control of the image generation process. The proposed method uses a transformer-like architecture operating pixel-wise, which receives the available labels as input tokens to merge them in a learned homogeneous space of labels. The merged labels are then used for image generation via conditional generative adversarial training. In this process, the sparsity of the labels is handled by simply dropping the input tokens corresponding to the missing labels at the desired locations, thanks to the proposed pixel-wise operating architecture. Our experiments on three benchmark datasets demonstrate the clear superiority of our method over the state-of-the-art and the compared baselines.

1 Introduction

In recent years, automated image generation under user control has become more and more of a reality. Such processes are typically based on so-called conditional image generation methods [34,21]. One could see these as an intermediate between fully unconditional [15] and purely rendering based [7] generation, respectively. Methods belonging to these two extreme cases either offer no user control (the former) or need to get all necessary information of image formation supplied by the user (the latter). In many cases, neither extreme is desirable. Therefore, several conditional image generation methods, that circumvent the rendering process altogether, have been proposed. These methods usually receive the image descriptions either in the form of text [34,45] or as spatially localized semantic classes [21,39,47].

^{*} Equal contributions.

In this paper, we aim to condition the image generation process beyond text descriptions and the desired semantics. In this regard, we make a generic practical assumption that any semantic or geometric aspects of the desired image may be available for conditioning. For example, an augmented reality application may require to render a known object using its 3D model and specified pose, but with missing texture and lighting details. In such cases, attributes such as semantic mask, depth, normal, curvature at that object’s location, become instantly available for the image generation process, offering us the multi-conditioning inputs. The geometric and semantic aspects of the other parts of the same image may also be available partially or completely. Incorporating all such information in a multi-conditional manner to generate the desired image, is the main challenge that we undertake. In some sense, our approach bridges the gap between generative and rendering based image synthesis.

Two major challenges of multi-conditional image generation, in the context of this paper, are the heterogeneity and the sparsity of the available labels. The heterogeneity refers to the difference in representation of different labels, for e.g. depth and semantics. On the other hand, the sparsity is either simply caused by the label definition (e.g. sky has no normal) or due to missing annotations [42]. It is important to note that some geometric aspects of images, such as an object’s depth and orientation, can be introduced manually (e.g. by sketching), without requiring any 3D model with its pose. This allows users to geometrically control images (beyond the semantics based control) both in the presence or absence of 3D models. It goes without saying that the geometric manipulation of any image can be carried out by first inferring its geometric attributes using existing methods [42,49,61], followed by generation after manipulation.

To address the problems of both heterogeneity and diversity, we propose a label merging network that learns to merge the provided conditioning labels pixel-wise. To this end, we introduce a novel transformer-based architecture, that is designed to operate on each pixel individually. The provided labels are first processed by label-specific multilayer perceptrons (MLPs) to generate a token for each label. The tokens are then processed by the transformer module. In contrast to popular vision transformers that perform spatial attention [9,62], our transformer module applies self-attention across the label dimension, thus avoiding the high computational complexity. The pixel-wise interaction of available labels homogenizes the different labels to a common representation for the output tokens. The output tokens are then averaged to obtain the fused labels in the homogeneous space to form the local *concept*. This is performed efficiently for all pixels in parallel by sliding the pixel-wise transformer over the input label maps. Finally, the concepts are used for the image generation via conditional generative adversarial training, using a state-of-the-art method [47]. During the process of label merging, the spatial alignment is always preserved. The sparsity of the labels is handled by simply dropping the input tokens of the missing labels, at the corresponding pixel locations. This way, the transformer learns to reconstruct the concept for each pixel, also in the case when not all labels are available.

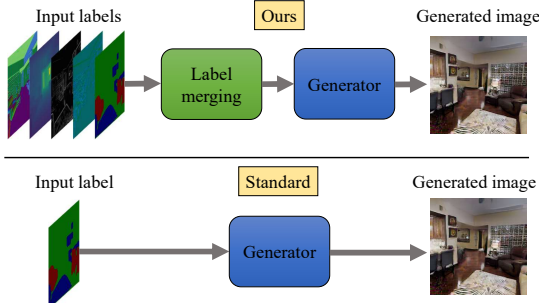


Fig. 1. **Spatially multi-conditional image generation.** Our model uses multiple labels to generate an image, compared to standard approaches which use only the semantic segmentation label. Multiple input labels, coming from different sources, are handled by the proposed label merging block.

We study the influence of several spatially conditioning labels including semantics, depth, normal, curvature, edges, in three different benchmark datasets. The influence of the labels is studied both the case of sparse and dense label availability. In both cases, the proposed method provides outstanding results by clearly demonstrating the benefit of conditioning labels beyond the commonly used image semantics. The major contribution of this paper can be summarized as follow:

1. We study the problem of spatially multi-conditional image generation, for the first time.
2. We propose a novel neural network architecture to fuse the heterogeneous multi-conditioning labels provided for the task at hand, while also handling the sparsity of the labels at the same time.
3. We analyse the utility of various conditioning types for image generation and present outstanding results obtained by the proposed method in benchmark datasets.

2 Related Work

Conditional Image Synthesis. A description of the desired image to be generated can be provided in various forms, from class conditions [35,3], text [34,45], spatially localized semantic classes [21,39,47], sketches [21], style information [13,23,24] to human poses [33]. Recently, the handling of different data structures (e.g. text sequences and images) has received attention in the literature [64,59]. The problem of spatially multi-conditional image generation is orthogonal to the problem of unifying different (non-spatial) modalities, as it seeks to fuse heterogeneous spatially localized labels into concepts, while preserving the spatial layout for image generation. In the area of image-to-image translation, Ronneberger

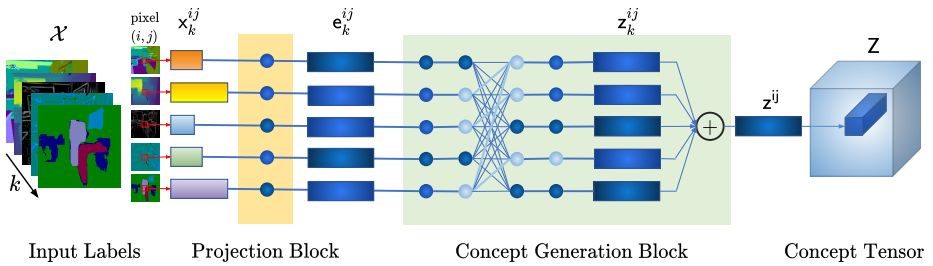


Fig. 2. **Pixel-wise Transformer Label Merging block (TLAM).** The heterogeneous labels of each pixel are first projected into the same dimensionality, and then passed to the concept generation block. A transformer module promotes the interaction between labels, before finally distilling them to a concept representation by averaging the homogeneous label embeddings at every pixel location.

et al. first introduced the *UNet* [46] architecture, which has been used in several important follow up works. Isola et al. [21] later introduced the *Pix2Pix* paradigm that leveraged the UNet backbone for a generator and combined it with a convolutional discriminator, to convert sketches into photo-realistic images. This work was improved by Wang et al. to support high resolution image translation in *Pix2PixHD* [57] and video translation in *Vid2Vid* [56]. Recently, Shaham et al. introduced the *ASAP-Net* [47] which achieves a superior trade-off of inference time and performance on several image translation tasks. We employ the *ASAP-Net* as one component in our architecture.

Conditioning Mechanisms. The conditioning mechanism is at the core of semantically controllable neural networks, and is often realized in conjunction with normalization techniques [10,19]. Perez et al. introduced a simple feature-wise linear modulation FiLM [41] for visual reasoning. In the context of neural style transfer [12], Huang et al. introduced Adaptive Instance Normalization AdaIN [20]. Park et al. extended AdaIN for spatial control in SPADE [39], where the normalization parameters are derived from a semantic segmentation. Zhu et al. [65] further extend SPADE to allow for independent application of global and local styles. Finally, generic normalisation schemes that make use of kernel prediction networks to achieve arbitrarily global and local control include Dynamic Instance Normalization (DIN) [22] and Adaptive Convolutions (AdaConv) [5]. While being greatly flexible, they also increase the resulting inference time, unlike ASAP-Net that uses adaptive implicit functions [48] for efficiency.

Differentiable Rendering Methods. Since rendering is a complex and computationally expensive process, several approximations were proposed to facilitate its use for training neural networks. Methods starting from simple approximations of the rasterization function to produce silhouettes [26,31,28] to more complex approximations modelling indirect lighting effects [29,37,32] have been proposed. These algorithms have also been incorporated into popular deep learning frameworks [44,29,38]. Differentiable renderers have been successfully

used in several neural networks including those used for face [52,51] and human body [30,40] reconstruction. We refer the interested reader to the excellent surveys of Tewari et al. [50] and Kato et al. [25] for more details. In contrast to rendering approaches which require setting numerous scene parameters, our method directly generates realistic images from only a sparse set of chosen labels.

3 Method

We start by introducing a few formal notations. As an input, we have a collection of labels $\mathcal{X} = \{X_1, X_2, \dots, X_N\}$, where each label $X_k \in \mathbb{R}^{H \times W \times C_k}$ has height H , width W and C_k channels. The element of the label X_k corresponding to the pixel location (i, j) is denoted as $x_k^{ij} \in \mathbb{R}^{C_k}$. Hence, elements of the label set \mathcal{X} corresponding to the pixel location (i, j) form a set $\mathcal{X}^{ij} = \{x_1^{ij}, x_2^{ij}, \dots, x_N^{ij}\}$. The model takes the set of labels \mathcal{X} as an input and produces $I = \phi(\mathcal{X})$, where $I \in \mathbb{R}^{H \times W \times 3}$ is the generated image.

3.1 Label Merging

We describe the mechanism of the label merging component, as illustrated in Figure 2. This component processes different spatial locations of the input labels \mathcal{X}^{ij} independently, and is efficiently performed on all pixels in parallel. We empirically found this to be sufficient. To this end, we first collapse the spatial dimensions of every label X_k to obtain $E_k \in \mathbb{R}^{HW \times d}$, which contains HW embedding vectors $e_k^{ij} \in \mathbb{R}^d$. In this process, we are interested to merge all embedding vectors $\{e_k^{ij}\}$ into a common concept vector z^{ij} , for each pixel location. The label merging is performed by two blocks: the projection block and the concept generation block, which we described in the following.

Projection Block This block projects every heterogeneous input label X_k into an embedding space $E_k \in \mathbb{R}^{H \times W \times d}$, where d is the dimensionality of the embedding space. It does so by transforming every token x_k^{ij} with the projection function f_k , to project it into the embedding space $e_k^{ij} = f_k(x_k^{ij})$, where $e_k^{ij} \in \mathbb{R}^d$. All the elements of a given label X_k share the same projection function f_k . Different input labels have different projection functions f_k . We use an affine transformation followed by the GeLU nonlinearity $a(\cdot)$ [17] to serve as the embedding function,

$$e_k^{ij} = f_k(x_k^{ij}) = a(A_k x_k^{ij} + b_k), \quad (1)$$

where $A_k \in \mathbb{R}^{d \times C_k}$ and $b_k \in \mathbb{R}^d$. We implement this by using fully connected layers as projection functions for each input label X_k , followed by the GeLU activation function. Our method also works with sparse input labels, which can be caused by label definition or missing labels. When the value of a label X_k is missing at a certain spatial location, its element token x_k^{ij} is dropped by setting it to a zero vector. Thus, a token with the embedding $e_k^{ij} = a(b_k)$ will send a signal to the concept generation block that the label k is not present at this

location, and that it should extract the information from other labels. Also, the absence of the whole label X_k is handled similarly.

Concept Generation Block The collection of the embedding vectors corresponding to different labels $\mathcal{E} = \{e_1, \dots, e_k, \dots, e_N\}$ serve as input tokens for our concept generation block. This block uses a novel attention mechanism to model the interaction across labels, which is shared across all spatial locations. It therefore does not require expensive spatial attention as used in vision transformer architectures [53,9]. In other words, we apply the same label-transformer on each pixel individually. Transformers are naturally suited here to encourage interaction between the embedded label tokens to share their label specific information while merging it into the final label representation. Before giving \mathcal{E} to the transformer, we add label specific encodings p_k to the embedded tokens e_k to obtain $z_k^{(0)} = e_k + p_k$. Then we pass $\mathcal{Z}^{(0)} = \{z_1^{(0)}, z_2^{(0)}, \dots, z_N^{(0)}\}$ through l transformer blocks B_m . Each block B_m takes the output $\mathcal{Z}^{(m-1)}$ of the previous block and produces $\mathcal{Z}^{(m)} = B_m(\mathcal{Z}^{(m-1)})$, where $\mathcal{Z}^{(m)} = \{z_1^{(m)}, z_2^{(m)}, \dots, z_N^{(m)}\}$.

Each transformer block B_m is composed of a Multi-head Self Attention block (MSA), followed by a Multilayer Perceptron block (MLP) [53,9]. Self-attention is a global operation, where every token interacts with every other token and thus information is shared across them. Multiple heads in the MSA block are used for more efficient computation and for extracting richer and more diverse features. The MSA block executes the following operations:

$$\hat{\mathcal{Z}}^{(m)} = \text{MSA}(\text{LN}(\mathcal{Z}^{(m-1)})) + \mathcal{Z}^{(m-1)}, \quad (2)$$

where LN represents Layer Normalization [2]. The MSA block is followed by the MLP block, which processes each token separately using the same Multilayer Perceptron. This block further processes the token features, after their global interactions in the MSA block, by sharing and refining the representations of each token across all their channels. The MLP block executes the following operations:

$$\mathcal{Z}^{(m)} = \text{MLP}(\text{LN}(\hat{\mathcal{Z}}^{(m)})) + \hat{\mathcal{Z}}^{(m)}. \quad (3)$$

Note that, for vision transformers [9] operating on M spatial elements (e.g. pixels/patches), the computational complexity of the self-attention is $\mathcal{O}(M^2)$. Our pixel-wise transformer, operating only on N label tokens, reduces the complexity of self-attention to $\mathcal{O}(N^2)$ (per pixel) with the number of labels $N \ll M$.

Finally, all the elements of the output set produced by the final transformer block $\mathcal{Z} = \{z_1^{(l)}, z_2^{(l)}, \dots, z_N^{(l)}\}$ are averaged to obtain $z = \frac{1}{N} \sum_{k=1:N} z_k$. They are reshaped back into the original spatial dimensions to obtain the *Concept Tensor* $Z \in \mathbb{R}^{H \times W \times d}$. We name this label merging block as the Transformer LAbel Merging (**TLAM**) block.

3.2 Network Overview

The proposed model is divided into two components: the label merging component and the image generation component. This is depicted in Figure 3.

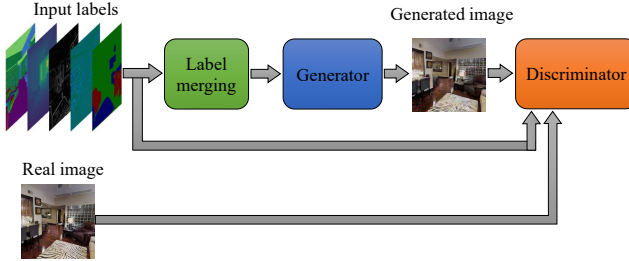


Fig. 3. **Network overview.** Different input labels are embedded into a homogeneous space with the label merging module. The generator uses this embedding to produce the output image. During training, the discriminator takes the input labels, real and generated images, and uses them to optimize the label merging and generator modules.

Label Merging. The label merging block takes the set of heterogeneous labels \mathcal{X} as the input and merges them into a homogeneous space $Z = \psi(\mathcal{X})$, where $Z \in \mathbb{R}^{H \times W \times d}$ is the *Concept Tensor*. It is important to note that the label merging block does not require the number of input labels to be the same for every input. Input labels \mathcal{X} are heterogeneous because they come from different sources and can have different numbers of channels C_k , as well as different ranges of values. For example, semantic segmentation labels are represented using discrete values, while surface normals are continuous. The label merging block first translates all the provided labels X_k into the same dimensional embeddings E_k , using the projection block. Then, it uses the concept generation block to translate embeddings E_k to the concept tensor Z . In short, the label merging block fuses the heterogeneous set of input labels \mathcal{X} into a homogeneous Concept Tensor Z . This block is depicted in Figure 2.

Generator. The task of the generator is to take the produced *Concept Tensor* Z and generate the image $I = g(Z)$, as shown in Figure 3. As the generator, we employ the state-of-the-art ASAP model [47]. This model first synthesizes the high-resolution pixels using lightweight and highly parallelizable operators. ASAP performs most computationally expensive image analysis at a very coarse resolution. We modify the input to ASAP, by providing the *Concept Tensor* Z as an input, instead of giving only one specific input labels X_k . The generator can therefore exploit the merged information from all available input labels \mathcal{X} .

Adversarial Training for Multi-conditioning. We follow the optimization protocol of ASAP-Net [47]. We train our generator model adversarially with a multi-scale patch discriminator, as suggested by pix2pixHD [57]. To achieve this, we modify the input to the discriminator by using the *Concept Tensor* Z instead of a specific label X_k , for example semantics used by the most existing works.

4 Experiments

Implementation Details. We follow the optimization protocol of ASAP-Net [47]. We train our generator model adversarially with a multi-scale patch discrimina-

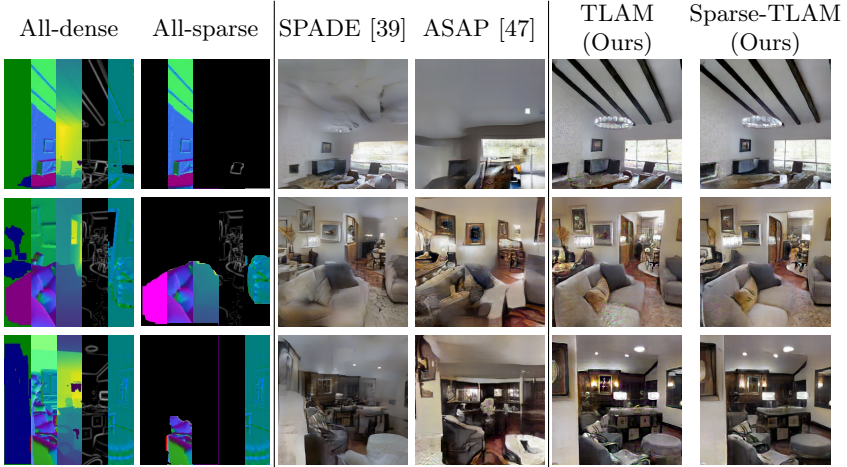


Fig. 4. **Visual comparisons on the Taskonomy dataset.** Column 1 & 2: five different labels tiled horizontally for dense and 50% sparse cases. Column 5 & 6: images generated by our method using the labels from column 1 & 2. Column 3 & 4: images generated by the dense semantic methods. Our method generates more realistic images with fine geometric and visual details from both dense and sparse labels.

| Backbone | Method | Label sparsity | | | | | FID |
|------------|----------------------|----------------|---|---|---|---|------|
| | | S | E | C | D | N | |
| SPADE [39] | Regular | ■ | | | | | 72.3 |
| | Naive-baseline | ■ | ■ | ■ | ■ | ■ | 66.1 |
| ASAP [47] | Regular | ■ | | | | | 73.8 |
| | Naive-baseline | ■ | ■ | ■ | ■ | ■ | 74.6 |
| | CLAM-baseline (Ours) | △ | △ | △ | △ | △ | 43.8 |
| | TLAM (Ours) | △ | △ | △ | △ | △ | 37.9 |
| | CLAM-baseline (Ours) | ■ | ■ | ■ | ■ | ■ | 37.1 |
| | TLAM (Ours) | ■ | ■ | ■ | ■ | ■ | 30.6 |

Table 1. **FID scores on the Taskonomy dataset.** Our TLAM method generates images with significantly better visual quality for both sparse and dense labels. Symbol ■ corresponds to dense labels, while △ corresponds to 50% label sparsity. S stands for semantics, E for edges, C for curvature, D for depth and N for normals. Please, refer Figure 4 for corresponding images.

tor, as suggested by pix2pixHD [57]. The training includes an adversarial hinge-loss, a perceptual loss and a discriminator feature matching loss. The learning rates for the generator and discriminator are 0.0001 and 0.0004, respectively. We use the ADAM [27] solver with $\beta_1 = 0$ and $\beta_2 = 0.999$, following [39,47]. To generate sparse labels, we look at spatial areas corresponding to distinct semantic segmentation instances. For the sparsity of S , we randomly drop the labels with $S\%$ probability, independently for every label inside every area. Please turn to the supplementary material for a detailed visualization of sparse labels.

4.1 Datasets

We conduct experiments on three different datasets to demonstrate the versatility and effectiveness of our approach.

Taskonomy dataset [63] is a multi-label annotated dataset of indoor scenes. The entire dataset consists of over 4 Million images from around 500 different buildings with high resolution RGB images, segmentation masks and other labels. We chose this dataset for our main experiments because of its wide selection of both semantic and geometric labels. In our experiments, we use the following labels: semantic segmentation, depth, surface normals, edges and curvature. We selected two buildings from the large dataset resulting a total of 18,246 images, split into 14,630/3,619 training/validation images.

Cityscapes dataset [8] contains images of urban street scenes from 50 different cities and their dense pixel annotations for 30 classes. The training and validation split contains 3000 and 500 samples respectively. To obtain further labels, we use a state-of-the art depth estimation network [14] for depth. The estimated depth, along with the camera intrinsics were used to compute the local patch-wise surface normals. Additionally, we use canny filters for edge detection. This resulted four labels for Cityscape.

NYU depth v2 dataset [36] consists of 1449 densely labeled pairs of aligned RGB images and depth, normals, semantic segmentation and edges maps of indoor scenes. We split the data into 1200/249 training/validation sets.

The presented qualitative and quantitative results are generated on the respective hold-out test sets, with the exception of Figure 9, where we follow the protocol of [57] for comparison with the other methods.

4.2 Baselines and Metrics

Since this is the first work for spatially multi-conditional image generation, we construct our own baselines.

Naive-baseline takes all the available inputs and concatenates them along the channel dimension to create the input, which is then fed as an input to the ASAP-Net or SPADE backbone. This also serves as an ablation to study the efficacy of the concept generation component in TLAM.

Convolutional Label Merging (CLAM-baseline) is another baseline that stacks multiple consecutive blocks similar to the projection block from Section 3.1. The first block is exactly the projection block (1), while the following l blocks perform the same operation with $A_k^l \in \mathbb{R}^{d \times d}$, $b_k^l \in \mathbb{R}^d$, preserving the dimensionality d . After the final block, all output elements corresponding to the same spatial location are averaged to produce the *Concept Tensor* Z , just like at the end of the TLAM block.

SotA semantic-only methods. We also compare our method with state-of-the-art semantic image synthesis models. These methods include SPADE [39], ASAP-Net [47], CRN [6], SIMS [43], Pix2Pix [21] and Pix2PixHD [57].

Performance Metrics. We follow the evaluation protocol of previous methods [47,39]. We measure the quality of generated images using the Fréchet Inception

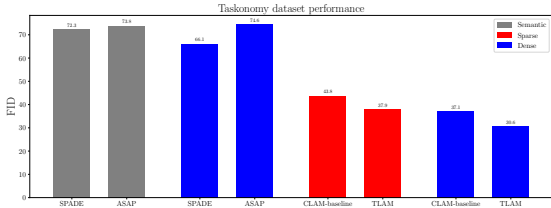


Fig. 5. Model comparison. Our TLAM method preforms better compared to the established baselines as well as to the SotA models which use semantic segmentation labels only.

Distance (FID) [18], which compares the distribution between generated data and real data. The FID summarizes how similar two groups of images are in terms of visual feature statistics. The second metric is the segmentation score, obtained by evaluating mean-Intersection-over-Union (mIoU) and pixel accuracy (accu) of a semantic segmentation model applied to the generated images. We use state-of-the-art semantic segmentation networks DRN-D-105 [60] for Cityscapes and DeepLabv3plus [4] for NYU depth v2 dataset.

4.3 Quantitative Results

Image Generation. Table 1 reports the FID scores obtained on the Taskonomy dataset. We compare our method with several baselines and with different label sparsity. Our TLAM significantly outperforms SPADE and ASAP SotA methods, which use only semantic segmentation maps as inputs. This shows that using different spatial input labels can indeed improve the generation quality. Moreover, when SPADE and ASAP merge multiple labels as an input, they do not perform significantly better than when using just the semantics. This emphasizes the difficulty of merging multiple spatial labels, which are heterogeneous in nature. Some labels represent semantic image properties, while others represent geometric properties. Also, some labels are continuous, while others are discrete. Furthermore, our TLAM performs better than the CLAM-baseline, showing the value of having a better label merging network to deal with the heterogeneity present in the input labels. Finally, we compare TLAM and the CLAM-baseline with dense and sparse labels. As expected, having dense labels achieves better image quality. The visual quality when using 50% sparse labels is close to when using dense labels. This is interesting and desirable, since in practical scenarios one often ends up having sparse labels [42].

The results on Cityscapes and NYU are summarized in Tables 2a and 2b. On the Cityscape dataset, we compare our method with the SotA methods and report FID, and segmentation mIoU and accuracy. Our method achieves better accuracy compared to the other methods. As reported in [39] the SIMS model produces a lower FID, but has poor segmentation accuracy on the Cityscapes. This is because SIMS synthesizes an image by first stitching image patches from the training dataset. On the NYU dataset, our method achieves better mIoU

and accuracy. Unfortunately, we are unable to report the FID, due to the small size of only 249 images in the validation set.

Training Convergence. Figure 6a shows the evolution of FID during training on Taskonomy. We evaluate the FID on the validation set every 20 epochs for TLAM, and the ASAP naive and CLAM baselines. One can observe that TLAM quickly achieves a very good FID, even after 20 epochs. At this instance, TLAM has 2.5 and 1.3 times better FID than those of the naive and CLAM baseline, respectively. We can also see that TLAM converges faster than the other models. One training epoch in Figure 6a takes about 1.7hrs for our method on one GeForce GTX TITAN X GPU.

4.4 Qualitative Results

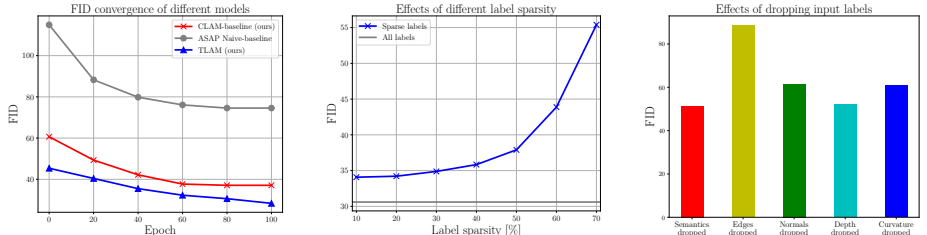
To visually compare our TLAM label merging, we present qualitative results for both dense and sparse labels on the Taskonomy dataset in Figure 4, together with semantic-only baselines. TLAM with all-dense and all-sparse labels generates high-fidelity images. Our method is able to generate fine structural details such as lights, decorations, and even mirror reflections clearly better than SPADE and ASAP. The results on the Cityscapes dataset are depicted in Figure 8. Notably, our method with sparse labels achieves similar visual quality as other methods. Figure 9 shows qualitative results on the NYU dataset, where Pix2PixHD also renders images with good quality. However, Pix2PixHD fails to capture the lighting conditions, in contrast to our method. Notably, our method captures the rich geometric structures (such as on the ceiling), thanks to the geometric labels. Please, refer to our supplementary material for more visual results. Overall, the qualitative results demonstrate the effectiveness of TLAM, which exploits novel pixel-wise label transformers, even for sparse labels.

4.5 Label Sensitivity Study

We analyse the sensitivity of our method with regards to the provided labels on the Taskonomy dataset.

Label Sparsity. Figure 6b shows how the FID is affected by label sparsity. Experiments conducted on increasing sparsity from 10% to 70%, show a steady degradation of FID with less available labels. *Note that our model already achieves good FID using only 30% of available labels.* The experiments were conducted using a single model trained with 50% sparsity. It also shows the generalizability of our method across various levels of sparsity.

Removal of Labels. In Figure 6c, we plot the FID after removing each label from the input, using the TLAM model trained on Taskonomy with 50% sparsity. We observe that among the five labels, edges play the most significant role. On the other hand, the semantics and depth are the most dispensable. Nevertheless, the removal of any label results into a worsening of the FID at least by a factor of 1.3. This suggests that all labels provide different information crucial for image generation, while being mutually complimentary.



(a) **Convergence of different models.** We compare FID scores during training of our TLAM method to the Naive and CLAM baselines. Our method converges faster and achieves better FID compared to those of the baselines at every point during training.

(b) **Effects of different label sparsity.** Our model achieves good FID score even when a fraction of labels is presented during inference. With more labels present, our model achieves better performance, even though it was trained for 50% label sparsity.

(c) **Effects of dropping input labels.** We examine how dropping a specific label affects the image quality of our TLAM model. Dropping any label degrades FID which leads to the conclusion that all labels provide useful information for image synthesis.

Fig. 6. **Training convergence and label sensitivity.** We analyse behavioural aspects of our models with regards to training and labels.

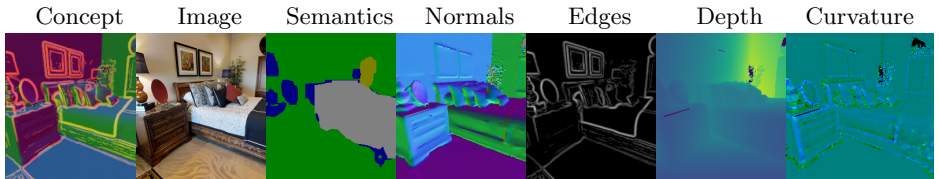


Fig. 7. **Concept Tensor visualization.** From left to right: *Concept Tensor* projected to RGB; original image; five different input labels.

We conclude that the proposed label merging block can successfully deal with incomplete labels and is able to exploit information from all available labels.

4.6 Concept Visualization and Image Editing

Concept Visualization. To visualize the concept tensor $Z \in \mathbb{R}^{H \times W \times 96}$, we project it to 3 channels, using Principal Component Analysis [11], and present it in Figure 7, along with the corresponding image and labels. One can observe that the visualized concept tensor indeed resembles different aspects of the input labels (e.g. edges and normal orientations).

Geometric Image Editing with User Inputs. In order to demonstrate an intuitive application of our method, we perform image editing by inserting a new object into the scene. Table 10 shows how our method can mimic rendering while allowing the geometric manipulation of an image. In this application, we render

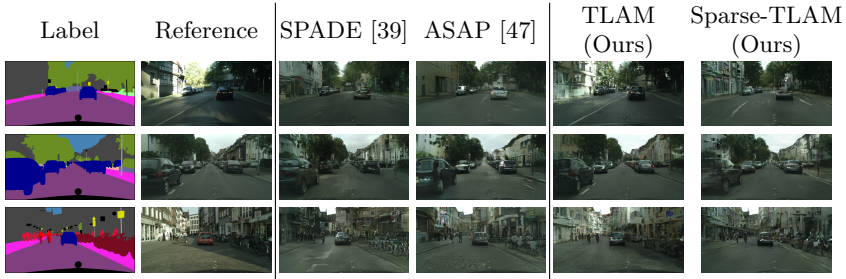


Fig. 8. **Visual comparison on the Cityscapes.** Our approach achieves a visual quality on par with the compared methods.



Fig. 9. **Visual comparison on NYU.** Our method generates images that better capture the lighting and geometry with more details.

a table in the given image, by simply augmenting different labels to include label information derived from a 3D model. Our method is able to render the table realistically within the image, while ASAP and SPADE perform unsatisfactorily. Figure 11 shows another example of inserting an object of interest into the image, as well as one example of removing a certain object from the image by augmenting the labels.

5 Conclusion

In this work, we offer a new perspective on image generation as inverse of image understanding. In the same way as image understanding involves the solving of multiple different tasks, we desire the control over the generation process to include multiple input labels of various kinds. To this end, we design a neural network architecture that is capable of handling sparse and heterogeneous labels, by mapping them to a homogeneous concept space in a pixel-wise fashion. With our proposed module, we can equip spatially conditioned generators with the desired properties. From our experiments on challenging datasets, we conclude that the benefits and flexibility of this additional layer of control gives way to exciting results beyond the state-of-the-art.

| Method | mIoU | Accuracy | FID |
|----------------|-------------|-------------|-------------|
| CRN [6] | 52.4 | 77.1 | 104.7 |
| SIMS [43] | 47.2 | 75.5 | 49.7 |
| Pix2Pix [21] | 39.5 | 78.3 | 80.7 |
| Pix2PixHD [57] | <u>58.3</u> | 81.4 | 95.0 |
| SPADE [39] | 62.3 | <u>81.9</u> | 71.8 |
| ASAP [47] | 44.9 | 78.6 | 72.5 |
| TLAM (Ours) | 45.5 | 85.3 | 68.3 |

(a) **Cityscapes dataset.** Our method is using the ASAP backbone.

| Method | mIoU | Accuracy |
|-------------|-------------|-------------|
| SPADE [39] | 33.1 | 47.4 |
| ASAP [47] | 36.2 | 49.1 |
| TLAM (Ours) | 38.3 | 53.1 |

(b) **NYU dataset.** Our method demonstrates effective of multi-conditioning with ASAP. Note that SPADE and ASAP are the SotA in semantic conditioning.

Table 2. **Quantitative results.** Our method enables successful multi-conditioning.

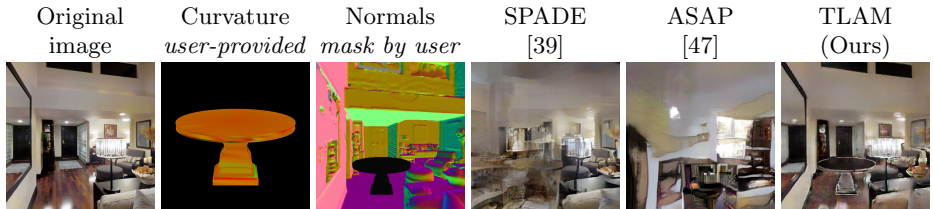


Fig. 10. **Geometric image editing with user inputs.** From left to right: original image; curvature label (provided among five) of the table to be inserted into the image; semantics of the table on the normal map of the scene; generated image using SPADE, ASAP and our method, respectively. During editing, we use dense labels of the original image, where we introduce five labels derived from a texture-less 3D model of a table (object of interest)– labels are first edited to introduce the object, followed by the image generation using the proposed TLAM method.



Fig. 11. **Object removal and insertion.** From left to right: original image; mask of the inserted/removed object; generated image using SPADE, ASAP and our method, respectively. Top row shows removal of chairs from the image, by removing their labels. Bottom row shows insertion of a TV, by inserting the labels provided by the user. The mask for removal/insertion is *manually* chosen by the user. Note that our TLAM generates consistent images, unlike the compared methods.

Spatially Multi-conditional Image Generation

Supplementary material

Ritika Chakraborty^{*1} Nikola Popovic^{*1}, Danda Pani Paudel¹,
Thomas Probst¹, Luc Van Gool^{1,2}

¹ Computer Vision Laboratory, ETH Zurich, Switzerland

² VISICS, ESAT/PSI, KU Leuven, Belgium

{critika, nipopovic, pauadel, probstt, vangoool}@vision.ee.ethz.ch

This document provides additional details, which complement the main paper. We provide the complete network diagram of our generator in Section A. More implementation details are contained in Section B. The visualization of input labels under different sparsity can be found in Section C. Additional qualitative results are presented in Section D. Finally, a discussion about ethical and societal impacts is contained in Section E. Also, please refer to our video supplementary for the example of geometric editing.

A Generator Overview

Whole Network. The network diagram of our generator is presented in Figure 1. The figure shows how our proposed Label Merging Block TLAM is connected to the ASAP-Net [47] generator, which we use as the backbone.

ASAP-Net Generator. The generator takes the *Concept Tensor* $Z \in \mathbb{R}^{H \times W \times d}$ as an input, similar to taking the semantic labels in the original design. It then outputs a tensor of weights, which parameterize the pixelwise spatially-varying multi-layer perceptrons (MLPs). The MLPs, with inferred weights, compute the final output image by taking the *Concept Tensor* Z as their input.

B Implementation Details

Projection Block. The Projection Block projects each input label into an embedding space with the same dimensionality. Every input label is processed by one 1x1 convolution layer, followed by a nonlinear activation. The projection is a 96-dimensional tensor for each label.

Concept generation Block. The Concept Generation Block takes the projected tensors as input, and operates over them in a pixel-wise fashion. For each pixel, we thus have an embedding vector for each task. We add a label specific-encoding to the embedding vector of each label, as a way of signalizing which task the embedding corresponds to. For every pixel, the concept generation block processes each set of encoded labels with a transformer. The transformer consists of 3 layers, where each uses 3 heads.

^{*} Equal contributions.

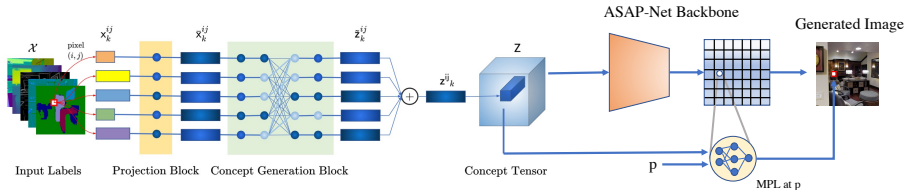


Fig. 1. Label Merging TLAM block and ASAP-Net Backbone. The input labels are processed by the label merging network to output the *Concept Tensor*. The ASAP generator takes the *Concept Tensor* $Z \in \mathbb{R}^{H \times W \times d}$ as an input and outputs a tensor of weights. Those weights are parameters of pixelwise, spatially-varying, MLPs, which compute the final output image from the *Concept Tensor* Z .

C Visualization of input Labels

In Figure 2 we show examples of the input labels from the Taskonomy dataset. These labels include semantic segmentation, normals, depth, edges and curvature. Furthermore, in Figure 3, 4 and 5 we show examples of labels from the Taskonomy dataset, with 70%, 50% and 30% label sparsity. To generate sparse labels, we look at spatial areas corresponding to distinct semantic segmentation instances. For the sparsity of S , we randomly drop the labels with $S\%$ probability, independently for every label inside every area. Higher sparsity means there is a higher probability that a semantic region will be masked out for all labels.

D Additional Qualitative Results

In Figure 6 we show images synthesized with our TLAM model using dense input labels (semantics, curvature, edges, normals and depth), on the Taskonomy dataset. In Figure 7 we show images synthesized with our TLAM model using sparse input labels (50% sparsity), on the Taskonomy dataset. Finally, Figure 8 shows additional visual comparison on the Cityscapes dataset, where we compare our TLAM and Sparse-TLAM methods with SPADE [39] and ASAP-Net [47].

E Ethical and Societal Impact

This work is going one step further into the image generation. While bringing great potential artistic value to the general public, such technology can be misused for fraudulent purposes. Despite the generated images looking realistic, this issue can be partially mitigated by learning-based fake detection [16,55,54].

In regards to limitations, our method is not designed with a particular focus on balanced representation of appearance and labels. Therefore, image generation may behave unexpected on certain conditions, groups of objects or people. We recommend application-specific strategies for data collection and training to ensure the desired outcome [1,58].

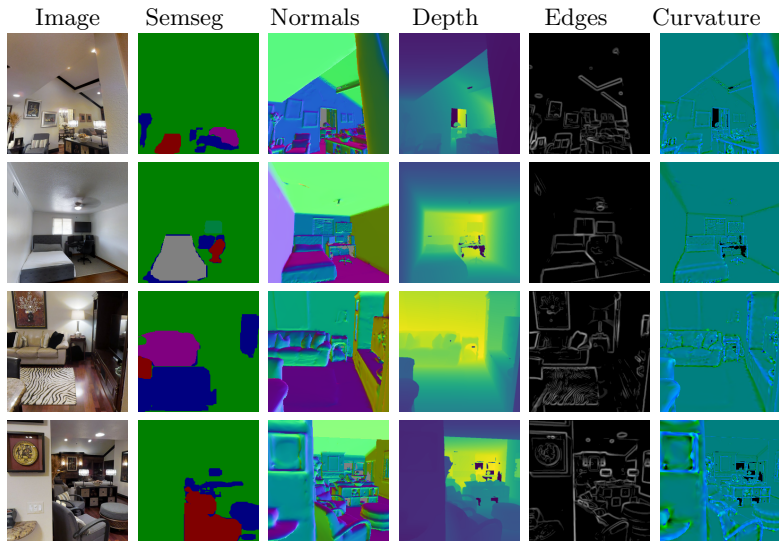


Fig. 2. **Examples of dense input labels.** Samples of the Taskonomy dataset with all input labels visualized.

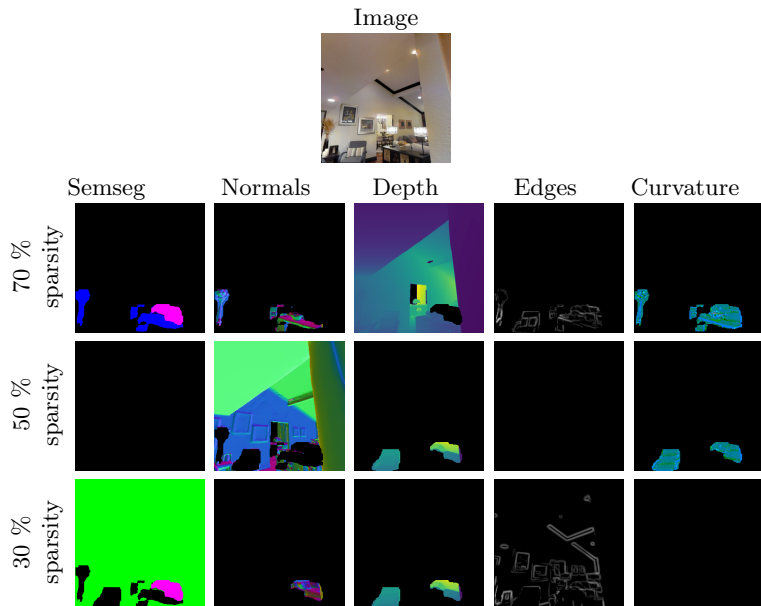


Fig. 3. **One example of sparse input labels.** One sample from the Taskonomy dataset where input labels have the sparsity of 70%, 50% and 30%.

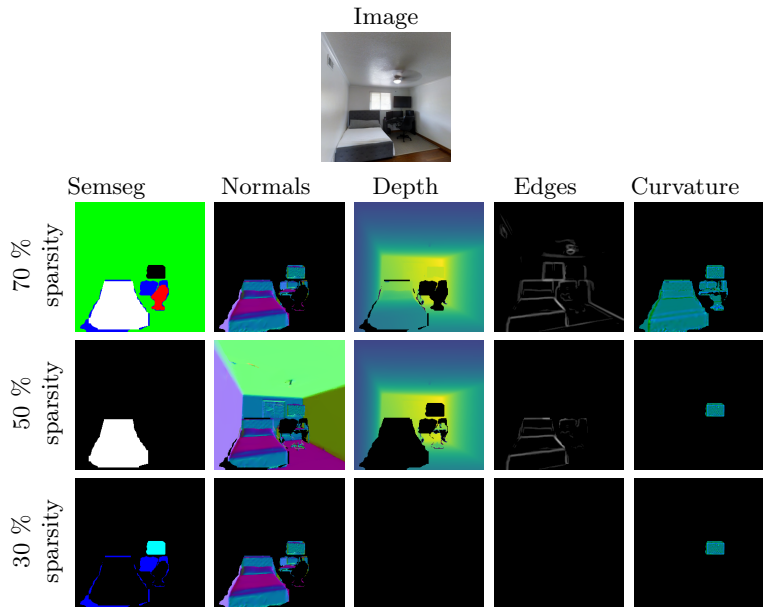


Fig. 4. **One example of sparse input labels.** One sample from the Taskonomy dataset where input labels have the sparsity of 70%, 50% and 30%.

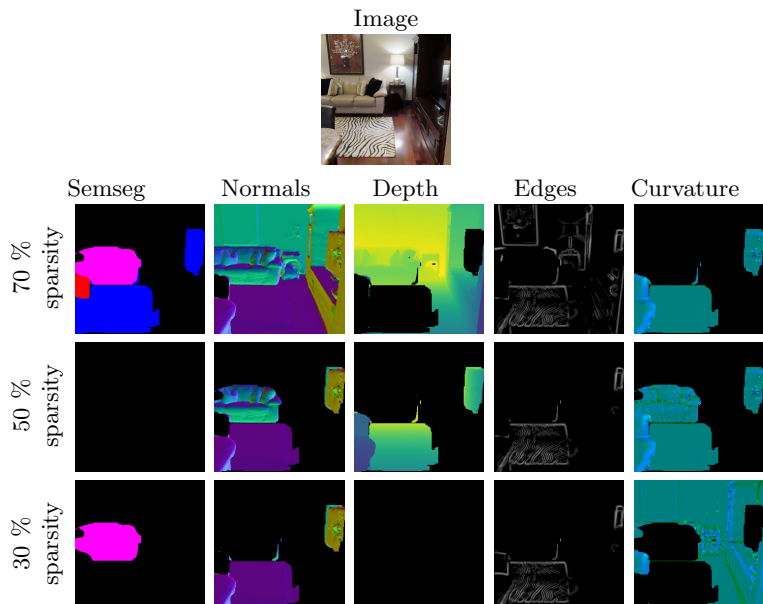


Fig. 5. **One example of sparse input labels.** One sample from the Taskonomy dataset where input labels have the sparsity of 70%, 50% and 30%.

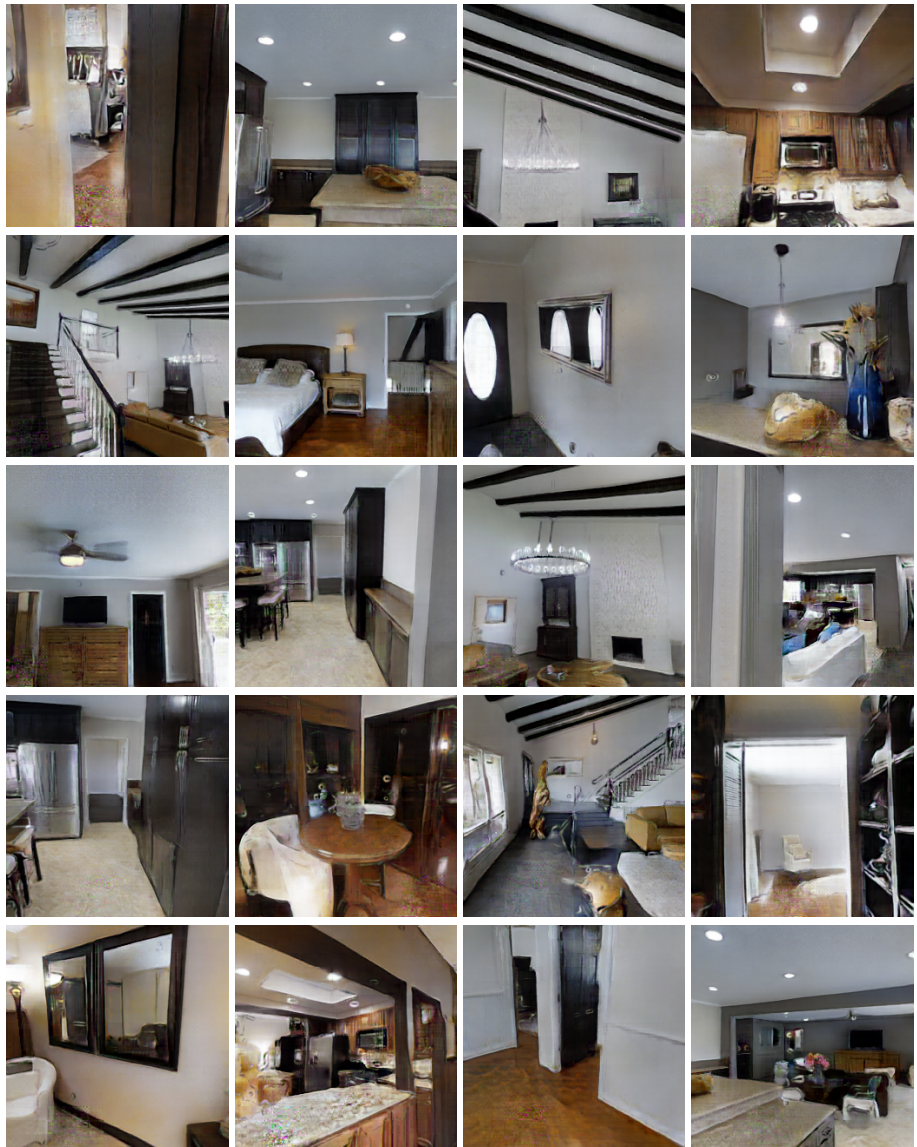


Fig. 6. **Images generated using dense input labels.** Here we see images generated with our proposed TLAM label merging model, using dense input labels from the Taskonomy dataset.

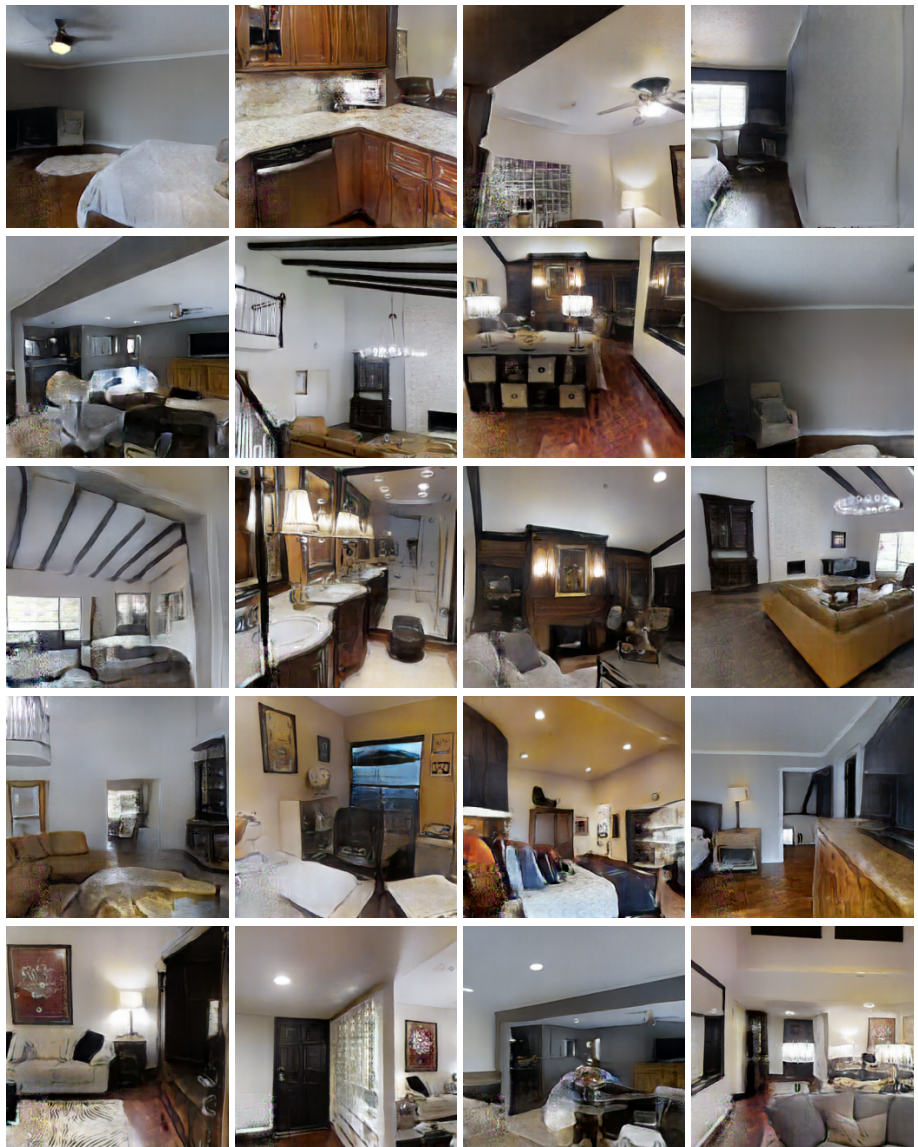


Fig. 7. **Images generated using 50% sparse input labels.** Here we see images generated with our proposed TLAM label merging model, using input labels from the Taskonomy dataset with 50% sparsity.

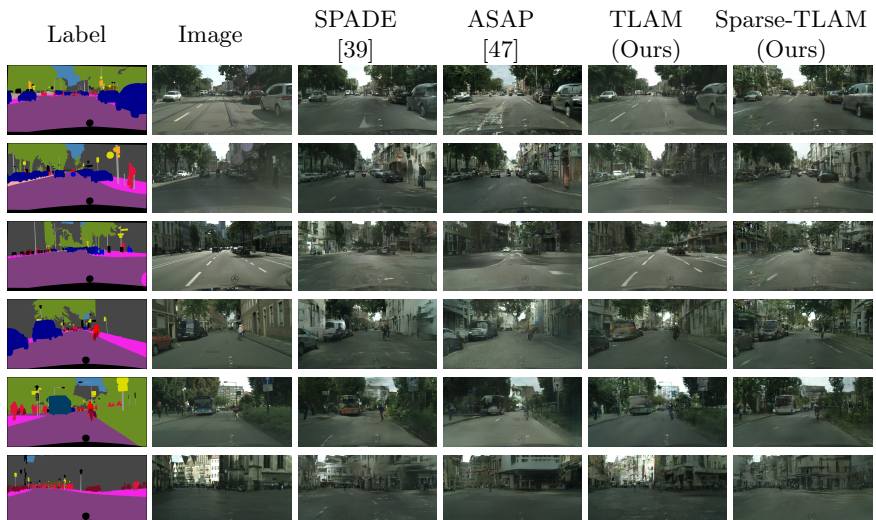


Fig. 8. **Image generation of different methods on Cityscapes.** Here we compare generated results of our methods TLAM and Sparse-TLAM to SPADE and ASAP-Net.

References

1. Alvi, M.S., Zisserman, A., Nelläker, C.: Turning a blind eye: Explicit removal of biases and variation from deep neural network embeddings. In: ECCV Workshops (2018)
2. Ba, J.L., Kiros, J.R., Hinton, G.E.: Layer normalization (2016)
3. Brock, A., Donahue, J., Simonyan, K.: Large scale gan training for high fidelity natural image synthesis. arXiv preprint arXiv:1809.11096 (2018)
4. Cao, J., Leng, H., Lischinski, D., Cohen-Or, D., Tu, C., Li, Y.: Shapeconv: Shape-aware convolutional layer for indoor rgb-d semantic segmentation. arXiv preprint arXiv:2108.10528 (2021)
5. Chandran, P., Zoss, G., Gotardo, P., Gross, M., Bradley, D.: Adaptive convolutions for structure-aware style transfer. In: Proceedings of the IEEE/CVF Conference on Computer Vision and Pattern Recognition (CVPR). pp. 7972–7981 (June 2021)
6. Chen, Q., Koltun, V.: Photographic image synthesis with cascaded refinement networks. pp. 1520–1529 (10 2017). <https://doi.org/10.1109/ICCV.2017.168>
7. Cook, R.L., Carpenter, L., Catmull, E.: The reyes image rendering architecture. ACM SIGGRAPH Computer Graphics **21**(4), 95–102 (1987)
8. Cordts, M., Omran, M., Ramos, S., Rehfeld, T., Enzweiler, M., Benenson, R., Franke, U., Roth, S., Schiele, B.: The cityscapes dataset for semantic urban scene understanding. In: Proceedings of the IEEE Conference on Computer Vision and Pattern Recognition (CVPR) (June 2016)
9. Dosovitskiy, A., Beyer, L., Kolesnikov, A., Weissenborn, D., Zhai, X., Unterthiner, T., Dehghani, M., Minderer, M., Heigold, G., Gelly, S., Uszkoreit, J., Houlsby, N.: An image is worth 16x16 words: Transformers for image recognition at scale. ICLR (2021)
10. Dumoulin, V., Perez, E., Schuchter, N., Strub, F., Vries, H.d., Courville, A., Bengio, Y.: Feature-wise transformations. Distill (2018). <https://doi.org/10.23915/distill.00011>
11. F.R.S., K.P.: Liii. on lines and planes of closest fit to systems of points in space. Philosophical Magazine Series 1 **2**, 559–572
12. Gatys, L.A., Ecker, A.S., Bethge, M.: A neural algorithm of artistic style (2015)
13. Gatys, L.A., Ecker, A.S., Bethge, M.: Image style transfer using convolutional neural networks. 2016 IEEE Conference on Computer Vision and Pattern Recognition (CVPR) pp. 2414–2423 (2016)
14. Godard, C., Mac Aodha, O., Brostow, G.J.: Unsupervised monocular depth estimation with left-right consistency. In: CVPR (2017)
15. Goodfellow, I., Pouget-Abadie, J., Mirza, M., Xu, B., Warde-Farley, D., Ozair, S., Courville, A., Bengio, Y.: Generative adversarial nets. Advances in neural information processing systems **27** (2014)
16. Guarnera, L., Giudice, O., Battiato, S.: Deepfake detection by analyzing convolutional traces. 2020 IEEE/CVF Conference on Computer Vision and Pattern Recognition Workshops (CVPRW) pp. 2841–2850 (2020)
17. Hendrycks, D., Gimpel, K.: Gaussian error linear units (gelus) (2020)
18. Heusel, M., Ramsauer, H., Unterthiner, T., Nessler, B., Hochreiter, S.: Gans trained by a two time-scale update rule converge to a local nash equilibrium. In: NIPS (2017)
19. Huang, L., Qin, J., Zhou, Y., Zhu, F., Liu, L., Shao, L.: Normalization techniques in training dnns: Methodology, analysis and application (2020)

20. Huang, X., Belongie, S.: Arbitrary style transfer in real-time with adaptive instance normalization. In: Proceedings of the IEEE International Conference on Computer Vision (ICCV) (Oct 2017)
21. Isola, P., Zhu, J.Y., Zhou, T., Efros, A.A.: Image-to-image translation with conditional adversarial networks. CVPR (2017)
22. Jing, Y., Liu, X., Ding, Y., Wang, X., Ding, E., Song, M., Wen, S.: Dynamic instance normalization for arbitrary style transfer (2019)
23. Johnson, J., Alahi, A., Fei-Fei, L.: Perceptual losses for real-time style transfer and super-resolution. In: Leibe, B., Matas, J., Sebe, N., Welling, M. (eds.) Computer Vision – ECCV 2016. pp. 694–711. Springer International Publishing, Cham (2016)
24. Karras, T., Laine, S., Aila, T.: A style-based generator architecture for generative adversarial networks (2019)
25. Kato, H., Beker, D., Morariu, M., Ando, T., Matsuoka, T., Kehl, W., Gaidon, A.: Differentiable rendering: A survey (2020)
26. Kato, H., Ushiku, Y., Harada, T.: Neural 3d mesh renderer. In: The IEEE Conference on Computer Vision and Pattern Recognition (CVPR) (2018)
27. Kingma, D.P., Ba, J.: Adam: A method for stochastic optimization. CoRR **abs/1412.6980** (2015)
28. Laine, S., Hellsten, J., Karras, T., Seol, Y., Lehtinen, J., Aila, T.: Modular primitives for high-performance differentiable rendering. ACM Transactions on Graphics **39**(6) (2020)
29. Li, T.M., Aittala, M., Durand, F., Lehtinen, J.: Differentiable monte carlo ray tracing through edge sampling. ACM Trans. Graph. (Proc. SIGGRAPH Asia) **37**(6), 222:1–222:11 (2018)
30. Lin, K., Wang, L., Liu, Z.: End-to-end human pose and mesh reconstruction with transformers (2021)
31. Liu, S., Li, T., Chen, W., Li, H.: Soft rasterizer: A differentiable renderer for image-based 3d reasoning (2019)
32. Loubet, G., Holzschuch, N., Jakob, W.: Reparameterizing discontinuous integrands for differentiable rendering. Transactions on Graphics (Proceedings of SIGGRAPH Asia) **38**(6) (Dec 2019). <https://doi.org/10.1145/3355089.3356510>
33. Ma, L., Jia, X., Sun, Q., Schiele, B., Tuytelaars, T., Gool, L.V.: Pose guided person image generation. In: NIPS (2017)
34. Mirza, M., Osindero, S.: Conditional generative adversarial nets. arXiv preprint arXiv:1411.1784 (2014)
35. Mirza, M., Osindero, S.: Conditional generative adversarial nets. ArXiv **abs/1411.1784** (2014)
36. Nathan Silberman, Derek Hoiem, P.K., Fergus, R.: Indoor segmentation and support inference from rgbd images. In: ECCV (2012)
37. Nimier-David, M., Speierer, S., Ruiz, B., Jakob, W.: Radiative back-propagation: An adjoint method for lightning-fast differentiable rendering. Transactions on Graphics (Proceedings of SIGGRAPH) **39**(4) (Jul 2020). <https://doi.org/10.1145/3386569.3392406>
38. Nimier-David, M., Vicini, D., Zeltner, T., Jakob, W.: Mitsuba 2: A retargetable forward and inverse renderer. Transactions on Graphics (Proceedings of SIGGRAPH Asia) **38**(6) (Dec 2019). <https://doi.org/10.1145/3355089.3356498>
39. Park, T., Liu, M.Y., Wang, T.C., Zhu, J.Y.: Semantic image synthesis with spatially-adaptive normalization (2019)
40. Pavlakos, G., Choutas, V., Ghorbani, N., Bolkart, T., Osman, A.A.A., Tzionas, D., Black, M.J.: Expressive body capture: 3d hands, face, and body from a single image (2019)

41. Perez, E., Strub, F., de Vries, H., Dumoulin, V., Courville, A.: Film: Visual reasoning with a general conditioning layer (2017)
42. Popovic, N., Paudel, D.P., Probst, T., Sun, G., Van Gool, L.: Compositetasking: Understanding images by spatial composition of tasks. In: Proceedings of the IEEE/CVF Conference on Computer Vision and Pattern Recognition. pp. 6870–6880 (2021)
43. Qi, X., Chen, Q., Jia, J., Koltun, V.: Semi-parametric image synthesis. pp. 8808–8816 (06 2018). <https://doi.org/10.1109/CVPR.2018.00918>
44. Ravi, N., Reizenstein, J., Novotny, D., Gordon, T., Lo, W.Y., Johnson, J., Gkioxari, G.: Accelerating 3d deep learning with pytorch3d. arXiv:2007.08501 (2020)
45. Reddy, M.D.M., Basha, M.S.M., Hari, M.M.C., Penchalaiah, M.N.: Dall-e: Creating images from text
46. Ronneberger, O., Fischer, P., Brox, T.: U-net: Convolutional networks for biomedical image segmentation (2015)
47. Rott Shaham, T., Gharbi, M., Zhang, R., Shechtman, E., Michaeli, T.: Spatially-adaptive pixelwise networks for fast image translation. In: Computer Vision and Pattern Recognition (CVPR) (2021)
48. Sitzmann, V., Zollhöfer, M., Wetzstein, G.: Scene representation networks: Continuous 3d-structure-aware neural scene representations. arXiv preprint arXiv:1906.01618 (2019)
49. Sun, G., Probst, T., Paudel, D.P., Popovic, N., Kanakis, M., Patel, J., Dai, D., Van Gool, L.: Task switching network for multi-task learning. In: Proceedings of the IEEE/CVF International Conference on Computer Vision. pp. 8291–8300 (2021)
50. Tewari, A., Fried, O., Thies, J., Sitzmann, V., Lombardi, S., Sunkavalli, K., Martin-Brualla, R., Simon, T., Saragih, J., Nießner, M., Pandey, R., Fanello, S., Wetzstein, G., Zhu, J.Y., Theobalt, C., Agrawala, M., Shechtman, E., Goldman, D.B., Zollhöfer, M.: State of the art on neural rendering (2020)
51. Tewari, A., Zollöfer, M., Bernard, F., Garrido, P., Kim, H., Perez, P., Theobalt, C.: High-fidelity monocular face reconstruction based on an unsupervised model-based face autoencoder. IEEE Transactions on Pattern Analysis and Machine Intelligence pp. 1–1 (2018). <https://doi.org/10.1109/TPAMI.2018.2876842>
52. Tewari, A., Zollöfer, M., Kim, H., Garrido, P., Bernard, F., Perez, P., Christian, T.: MoFA: Model-based Deep Convolutional Face Autoencoder for Unsupervised Monocular Reconstruction. In: The IEEE International Conference on Computer Vision (ICCV) (2017)
53. Vaswani, A., Shazeer, N.M., Parmar, N., Uszkoreit, J., Jones, L., Gomez, A.N., Kaiser, L., Polosukhin, I.: Attention is all you need. ArXiv **abs/1706.03762** (2017)
54. Verdoliva, L.: Media forensics and deepfakes: An overview. IEEE Journal of Selected Topics in Signal Processing **14**, 910–932 (2020)
55. Wang, S., Wang, O., Zhang, R., Owens, A., Efros, A.A.: Cnn-generated images are surprisingly easy to spot... for now. 2020 IEEE/CVF Conference on Computer Vision and Pattern Recognition (CVPR) pp. 8692–8701 (2020)
56. Wang, T.C., Liu, M.Y., Zhu, J.Y., Liu, G., Tao, A., Kautz, J., Catanzaro, B.: Video-to-video synthesis. In: Advances in Neural Information Processing Systems (NeurIPS) (2018)
57. Wang, T.C., Liu, M.Y., Zhu, J.Y., Tao, A., Kautz, J., Catanzaro, B.: High-resolution image synthesis and semantic manipulation with conditional gans. In: Proceedings of the IEEE Conference on Computer Vision and Pattern Recognition (2018)

58. Wang, Z., Qinami, K., Karakozis, Y., Genova, K., Nair, P.Q., Hata, K., Russakovsky, O.: Towards fairness in visual recognition: Effective strategies for bias mitigation. 2020 IEEE/CVF Conference on Computer Vision and Pattern Recognition (CVPR) pp. 8916–8925 (2020)
59. Xia, W., Yang, Y., Xue, J., Wu, B.: Tedigan: Text-guided diverse face image generation and manipulation. 2021 IEEE/CVF Conference on Computer Vision and Pattern Recognition (CVPR) pp. 2256–2265 (2021)
60. Yu, F., Koltun, V., Funkhouser, T.: Dilated residual networks. In: Computer Vision and Pattern Recognition (CVPR) (2017)
61. Yu, Y., Smith, W.A.: Inverserendernet: Learning single image inverse rendering. In: Proceedings of the IEEE/CVF Conference on Computer Vision and Pattern Recognition. pp. 3155–3164 (2019)
62. Yuan, L., Chen, Y., Wang, T., Yu, W., Shi, Y., Tay, F.E.H., Feng, J., Yan, S.: Tokens-to-token vit: Training vision transformers from scratch on imagenet. 2021 IEEE/CVF International Conference on Computer Vision (ICCV) pp. 538–547 (2021)
63. Zamir, A.R., Sax, A., Shen, W.B., Guibas, L.J., Malik, J., Savarese, S.: Taskonomy: Disentangling task transfer learning. In: IEEE Conference on Computer Vision and Pattern Recognition (CVPR). IEEE (2018)
64. Zhang, Z., Ma, J., Zhou, C., Men, R., Li, Z., Ding, M., Tang, J., Zhou, J., Yang, H.: M6-ufc: Unifying multi-modal controls for conditional image synthesis. arXiv preprint arXiv:2105.14211 (2021)
65. Zhu, P., Abdal, R., Qin, Y., Wonka, P.: Sean: Image synthesis with semantic region-adaptive normalization. In: Proceedings of the IEEE/CVF Conference on Computer Vision and Pattern Recognition (CVPR) (June 2020)